

A numerical study of three-dimensional natural convection in a differentially heated cubical enclosure

T. FUSEGI,^{†¶} J. M. HYUN,[‡] K. KUWAHARA[§] and B. FAROUK^{||}

[†] Institute of Computational Fluid Dynamics, 1-22-3 Haramachi, Meguro, Tokyo 152, Japan

[‡] Department of Mechanical Engineering, Korea Advanced Institute of Science and Technology, Chong Ryang, Seoul 131, Korea

[§] Institute of Space and Astronautical Science, 3-1-1 Yoshinodai, Sagamihara, Kanagawa 229, Japan

^{||} Department of Mechanical Engineering and Mechanics, Drexel University, Philadelphia, PA 19104, U.S.A.

(Received 19 June 1990 and in final form 31 July 1990)

Abstract—A high-resolution, finite difference numerical study is reported on three-dimensional steady-state natural convection of air, for the Rayleigh number range $10^3 \leq Ra \leq 10^6$, in a cubical enclosure, which is heated differentially at two vertical side walls. The details of the three-dimensional flow and thermal characteristics are described. Extensive use is made of state-of-the-art numerical flow visualizations. The existence of the transverse z -component velocity, although small in magnitude, is clearly shown. Comparison of the present three-dimensional results with the two-dimensional solutions is conducted. The three-dimensional data demonstrate reasonable agreement with the experimental measurements.

INTRODUCTION

NATURAL convection flow analysis in enclosures has many thermal engineering applications, such as cooling of electronic devices, energy storage systems and compartment fires. In the present paper, a numerical study is reported on steady-state three-dimensional natural convection in an air-filled cubical enclosure, which is heated differentially at two vertical side walls. As shown in Fig. 1, the temperature of the right vertical side wall (at $x = L_0$) is T_H , and that of the left side wall ($x = 0$) is T_C , where $T_H > T_C$. The remaining four walls are thermally insulated. The present geometry and the boundary conditions are mathematically well posed and they provide a basic model for relevant thermal engineering systems.

Two-dimensional numerical analyses for a square cavity filled with air have been carried out in the past over a wide range of Rayleigh numbers. Results for $10^3 \leq Ra \leq 10^6$ were presented in Markatos and Pericleous [1]. The laminar flow regime was assumed up to the Rayleigh number of 10^6 , and for higher Rayleigh numbers, the k - ϵ turbulence model was used. For $10^3 \leq Ra \leq 10^6$ and a Boussinesq fluid of $Pr = 0.71$, a set of benchmark solutions has been suggested by de Vahl Davis [2]. By resorting to systematic grid refinement practise and by concurrent use of the Richardson extrapolation to obtain grid-independent data, these solutions were claimed to be within an accuracy of 1%.

In order to simulate practical situations, three-dimensional flow calculations are highly desirable.

Three-dimensional laminar flows have been studied for enclosures of the depth aspect ratio, A_z , varying from 2 to 4 [3, 4]. Gross features observed in the enclosures revealed highly three-dimensional structures of the flow. The enclosures with $A_z = 1$ and 2 were considered in Lankhorst and Hoogendoorn [5]; they were computed for three Rayleigh numbers: $Ra = 10^6$, 4×10^8 and 10^{10} . In the last two cases, the k - ϵ turbulence model was employed. However, it is emphasized that these previous calculations were executed by using relatively coarse finite difference meshes, of up to $45 \times 45 \times 20$.

The present investigation is implemented on a much finer mesh system with a view toward delineating steady-state three-dimensional structures of the fields with sufficient resolution. The numerical resolution in the present three-dimensional calculations is comparable to the highest one among the preceding two-dimensional results [2]. The Rayleigh number ranges from 10^3 to 10^6 . The Prandtl number of the fluid is held fixed at 0.71. Comprehensive details of the flow and temperature fields are presented by displaying elaborate three-dimensional color graphics and illustrative field quantities. By inspecting these results of the realistic three-dimensional calculations, the validity of the prior two-dimensional results can be also assessed.

The majority of the past experimental works have studied high aspect ratio enclosures (e.g. $A \geq 5$), but relatively little research endeavor has been devoted to the cases of small aspect ratio cavities [6-11]. In most of these experimental investigations, care was taken to justify the two-dimensional approximation. Depth aspect ratios, A_z , greater than 5 were adopted in refs. [6-8] in an effort to minimize the end effect of the finite

[¶] Author to whom all correspondence should be addressed.

niques, will enable us to implement the three-dimensional numerical simulations of the flow and heat transfer properties in the enclosure. These numerical results will allow proper verification of the experimental observations. It is also noteworthy that, by cross-checking the results, the extent of the applicability of the earlier two-dimensional results to actual three-dimensional systems will be illuminated.

MATHEMATICAL MODEL

The flow field is described by the incompressible Navier–Stokes equations and the energy equation. The Boussinesq approximation is invoked for the fluid properties. The non-dimensionalized form of the governing equations can be expressed in tensor notation as

$$\frac{\partial u_i}{\partial x_j} = 0 \tag{1}$$

$$\frac{\partial u_i}{\partial t} + \frac{\partial}{\partial x_j} (u_j u_i) = - \frac{\partial p}{\partial x_i} + \frac{1}{Re} \frac{\partial^2 u_i}{\partial x_j \partial x_j} + \delta_{i2} \frac{T-1}{Fr} \tag{2}$$

$$\frac{\partial T}{\partial t} + \frac{\partial}{\partial x_j} (u_j T) = \frac{1}{Re Pr} \frac{\partial^2 T}{\partial x_j \partial x_j} \tag{3}$$

where δ_{ij} is the Kronecker delta ($\delta_{ij} = 1$ if $i = j$, and $\delta_{ij} = 0$ otherwise). The viscous dissipation and the pressure work terms are neglected in the energy equation.

The physical quantities are non-dimensionalized in the following manner:

$$(x, y, z) = (x^*, y^*, z^*)/L_0, \quad (u, v, w) = (u^*, v^*, w^*)/u_0, \\ t = t^* u_0 / L_0, \quad p = (p^* - p_0) / \rho^* u_0^2, \quad T = T^* / T_0$$

where an asterisk (*) denotes dimensional values. The reference scales for length, velocity, pressure and temperature are the enclosure height (L_0), the convective velocity ($u_0 = [g^* \beta^* L_0 (T_H - T_C)]^{1/2}$), the hydrostatic pressure (p_0) and the film temperature ($T_0 = (T_C + T_H)/2$), respectively. In the present non-dimensionalization, the Rayleigh, Prandtl and Reynolds numbers are related as $Ra = Re^2 Pr$. The Prandtl number is held fixed at 0.71 for air in the present study.

The boundary conditions are

$$u = v = w = 0 \quad \text{on all the walls} \tag{4}$$

$$T = (2 - \delta)/2 \text{ at } x = 0, \quad T = (2 + \delta)/2 \text{ at } x = 1,$$

$$\text{and } \partial T / \partial n = 0 \text{ at } y = 0, 1 \text{ and } z = 0, 1 \tag{5}$$

where n indicates the coordinate normal to the surface. The overheat ratio, δ , is set equal to 0.1 in the present analysis.

SOLUTION METHOD

A discretized form of the governing equations (1)–(3) is secured by a control-volume based finite differ-

ence procedure. Numerical solutions are acquired by an iterative method, together with the pressure correction algorithm, SIMPLE [12]. The present technique employs the Strongly Implicit Scheme (SIP) [13] to accelerate convergence characteristics of the solutions. SIP is applied to the planes of constant z in order to determine simultaneously the dependent variables in the x - and y -directions on each plane.

The convection terms in the momentum equation (2) are treated by the QUICK methodology [14, 15]. The QUICK scheme involves a third-order accurate upwind differencing, which possesses the stability of the first-order upwind formula and is free from substantial numerical diffusion experienced with the usual first-order techniques. In the present numerical procedure, a non-uniform grid version is adopted. The convection terms in the energy equation (3) are dealt with by a hybrid scheme [12].

The entire enclosure constitutes the full computational domain. The number of grid points for computations is $62 \times 62 \times 62$, except for the case of $Ra = 10^3$, in which a $32 \times 32 \times 32$ mesh network is chosen. Variable grid spacing is introduced to resolve steep gradients of the velocity and the temperature near the walls. The configuration of non-uniform grid systems is determined with the aid of parallel two-dimensional computations. The predictions of these two-dimensional computations have been satisfactorily compared with the benchmark solutions of de Vahl Davis [2]. The mesh distribution was altered systematically until the differences in the maximum velocity and the average Nusselt number at the isothermal walls fell less than 3 and 1.5%, respectively, of the reference data [2] at $Ra = 10^6$. Differences of less than 1% were achieved for the lower Rayleigh numbers.

The grid independency of the solutions has been confirmed at $Ra = 10^6$ by a test computation in which the number of grid points in the x -direction was doubled. This was done because the maximum gradients of the fields occur in the x -direction, in particular, within the boundary layers along the isothermal walls. Changes in the maximum velocities are approximately 2% as the number of grid points varied. The variance in the average Nusselt number at the isothermal walls was even smaller, i.e. less than 0.2%. When the Rayleigh number is lower, the differences are anticipated to decrease further.

Convergence of computations is declared when the following convergence criterion is satisfied:

$$\frac{|\phi_n - \phi_{n-1}|}{|\phi_n|_{\text{maximum}}} \leq 10^{-4} \text{ for all } \phi \tag{6}$$

where ϕ represents any dependent variable, and n refers to the value of ϕ at the n th iteration level.

At each Rayleigh number, the converged solution for a lower Rayleigh number is used as the initial guess. In actual computations, transient calculations

are conducted by an implicit method to generate steady-state solutions.

RESULTS AND DISCUSSION

Steady states were reached for all the Rayleigh numbers studied. Computations were performed on a HITACHI S-820/80 supercomputer system at the Institute of Computational Fluid Dynamics (ICFD) in Tokyo, Japan. The system has a maximum CPU speed of 3 GFLOPS and a maximum core memory of 512 MB. A typical computation required CPU time of 30 min with 600 iterations and 100 MB of memory. The three-dimensional graphics were produced by an interactive graphic software [16], which runs on a FUJITSU VP-200 supercomputer system at the ICFD.

The global field characteristics are examined by viewing comprehensive three-dimensional contours of the temperature and flow fields. Results for two Rayleigh numbers are inspected in detail in the following two subsections: $Ra = 10^4$ and 10^6 . The former case exemplifies a flow field in which the relative importance of convection is generally less significant. However, the latter case is representative of the flow structure in which convection is intense such that distinct boundary layers are discernible near the isothermal solid walls.

The case of $Ra = 10^4$

The isotherm surfaces are depicted in Fig. 2. The overall isotherm patterns on the constant z -planes are qualitatively similar to those of the two-dimensional flows; however, three-dimensional variations in the z -direction are also notable. As previously stated, the entire flow field constitutes the computational domain. The right half domain in $0.5 < z < 1$ is symmetric to the left half ($0 < z < 0.5$) with respect to the plane of $z = 0.5$. In addition, the flow on each constant z -plane is centro-symmetric with respect to the center of the cavity, ($x = 0.5, y = 0.5$). The three-dimensional variations in the z -direction, although generally weak in magnitude, are noticed in Fig. 2.

Figure 3 displays isosurfaces of constant velocities for each component (u, v and w). As can be inferred from the knowledge of two-dimensional flows, the x -component velocity (u), which constitutes the main flow, is concentrated in the regions near the horizontal walls ($y = 0$ and 1). Similarly, the y -component velocity (v) has large values near the isothermal vertical walls ($x = 0$ and 1). Combining these descriptions, the bulk of the enclosure is occupied principally by a single cell. As is clear in Figs. 3(a) and (b), the three-dimensionalities in the main streams (u and v fields) are less conspicuous in much of the interior region. Figure 3(c) illustrates the transverse velocity component (w). Note that w is, in general, an order of magnitude smaller than the dominant main stream flows (u and v). It should be pointed out that w vanishes at the end walls ($z = 0$ and 1) and at the mid-

symmetry plane ($z = 0.5$). The transverse flows, which are noticeable in the enclosure, are a direct manifestation of the three-dimensional nature of the flow.

Another physical variable, which is informative in depicting the gross flow field characteristics, is the vorticity. Figure 4 illustrates the absolute value of the vorticity, which is defined as the magnitude of the vorticity vector. This figure gives a direct indication of the velocity gradients. As is clearly demonstrated in Fig. 4, the gradients of flow are substantial in narrow regions in the vicinity of the solid boundary walls. The plots of the isovorticity surfaces also reflect the existence of a dominant unicellular structure in much of the enclosure.

The case of $Ra = 10^6$

The computed results at this high Rayleigh number are characterized by a combination of the distinct boundary layers near the side walls ($x = 0$ and 1) and the almost stagnant interior core. These are clearly captured in the isotherm surfaces shown in Fig. 5. The existence of the thin boundary layers on the vertical isothermal walls, and of the near-linear temperature stratification in the interior, is evident. The three-dimensional variations are noticeable very near the end walls ($z = 0$ and 1).

The regions of large velocities (u and v) are now confined into the areas near the walls, as revealed in Figs. 6(a) and (b). Notice that, in comparison to the case of $Ra = 10^4$ (see Fig. 3), the concentration of dominant flows is more pronounced and the boundary layer thickness is smaller at this Rayleigh number. The z -variations of the flows are appreciable, especially near the solid walls. In particular, as can be noted in Fig. 6(c), strong transverse flows (w) are generated near the corners. The transverse velocity component is again found to be one order of magnitude lower than the dominant velocity components (u and v).

The contours of the absolute magnitude of the vorticity, shown in Fig. 7, clearly demonstrate again the combined structure of the distinct boundary layers and the near-stagnant interior core. Three-dimensionalities are prominent only near the end walls; this is similar to the behavior of the temperature field discussed earlier. It is noteworthy that areas of weak vortices are found in the regions where the isothermal vertical side walls ($x = 0$ and 1) abut the adiabatic vertical end walls ($z = 0$ and 1). These regions extend over the entire height of the enclosure. The presence of these secondary vortices has also been documented by the numerical simulations of Lankhorst and Hoogendoorn [5], who dealt with an enclosure of aspect ratio, A_z , of 2.

Heat transfer characteristics

The non-dimensionalized heat transfer rate at the isothermal walls is represented by the Nusselt numbers. These quantities are defined as follows:

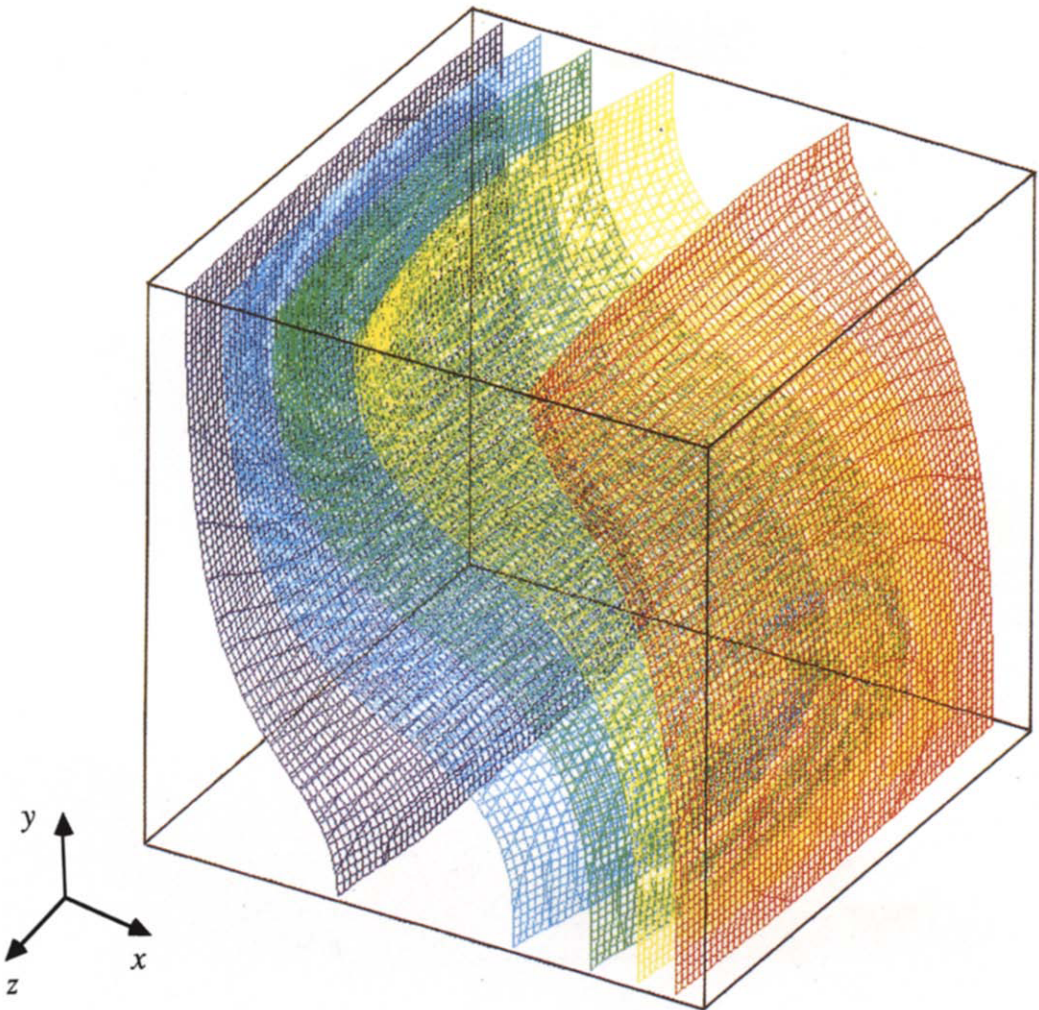


FIG. 2. The temperature field at $Ra = 10^4$ (contour levels : 0.9667 (purple), 0.9833 (blue), 1.0 (green), 1.017 (yellow), 1.033 (red)).

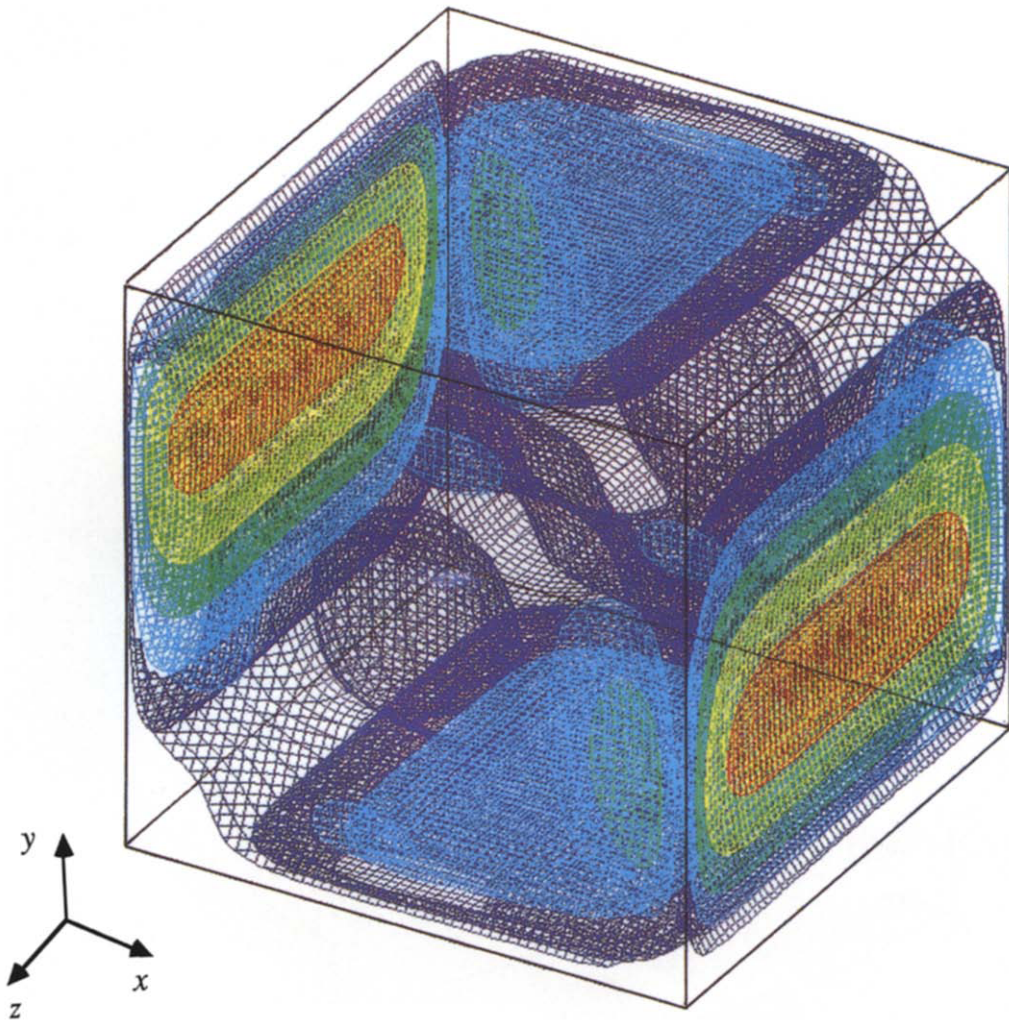


FIG. 4. Isosurfaces of the absolute values of the vorticity at $Ra = 10^4$ (contour levels: 0.9 (purple), 1.8 (blue), 2.7 (green), 3.6 (yellow), 4.5 (red)).

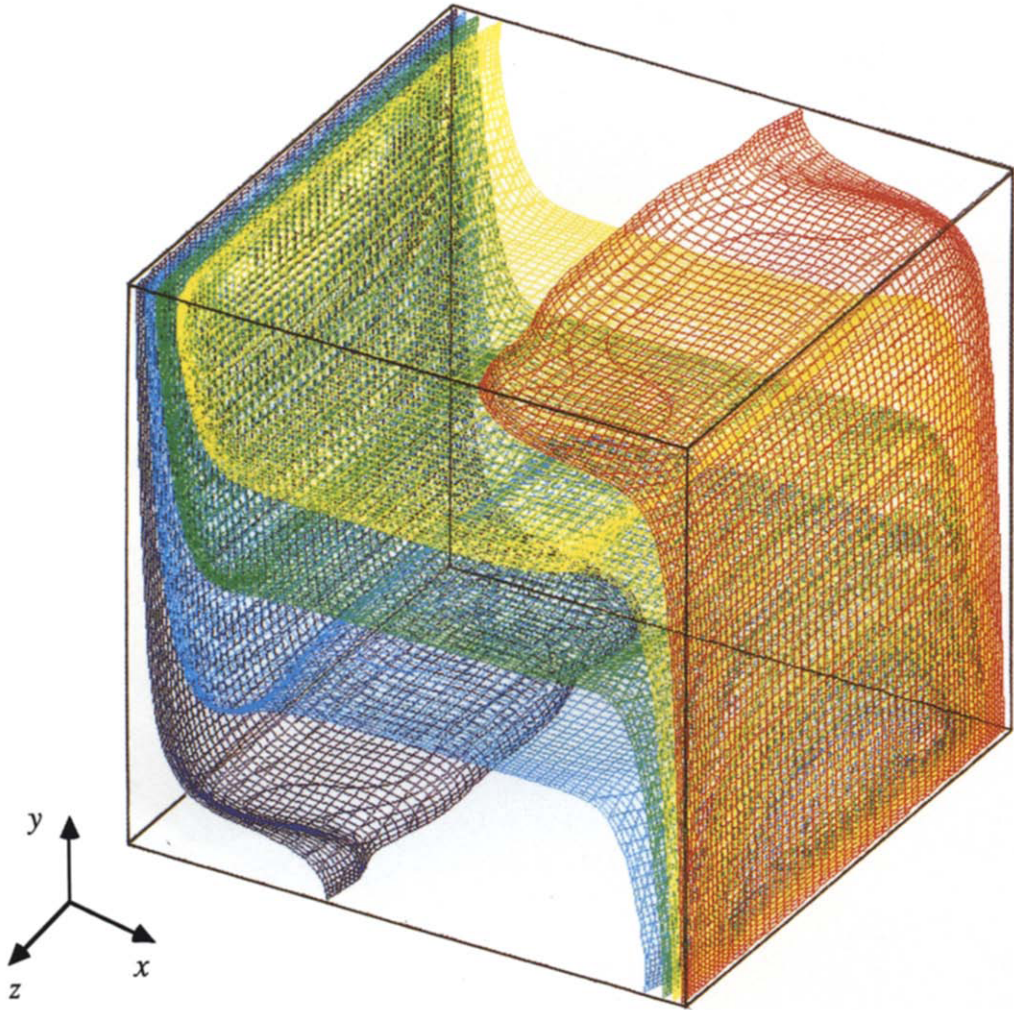
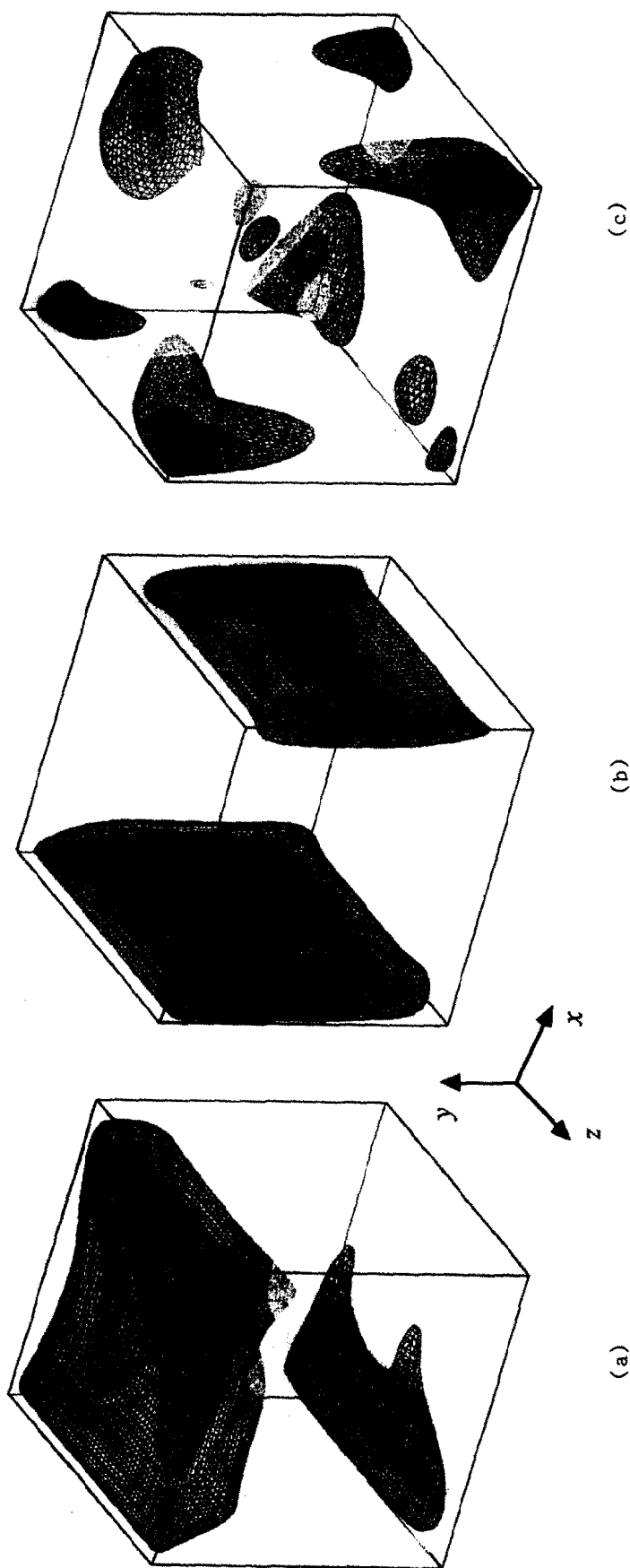


FIG. 5. The temperature field at $Ra = 10^6$ (contour levels : 0.9667 (purple), 0.9833 (blue), 1.0 (green), 1.017 (yellow), 1.033 (red)).



(a) u -Velocity components (contour levels: -0.18 (purple), -0.12 (blue), -0.06 (green), 0.06 (yellow), 0.12 (pink), 0.18 (red)). (b) v -Velocity components (contour levels: -0.3 (red), 0.1 (green), 0.1 (yellow), 0.2 (pink), 0.3 (red)). (c) w -Velocity components (contour levels: -0.036 (purple), -0.024 (blue), -0.012 (green), 0.012 (yellow), 0.024 (pink), 0.036 (red)).

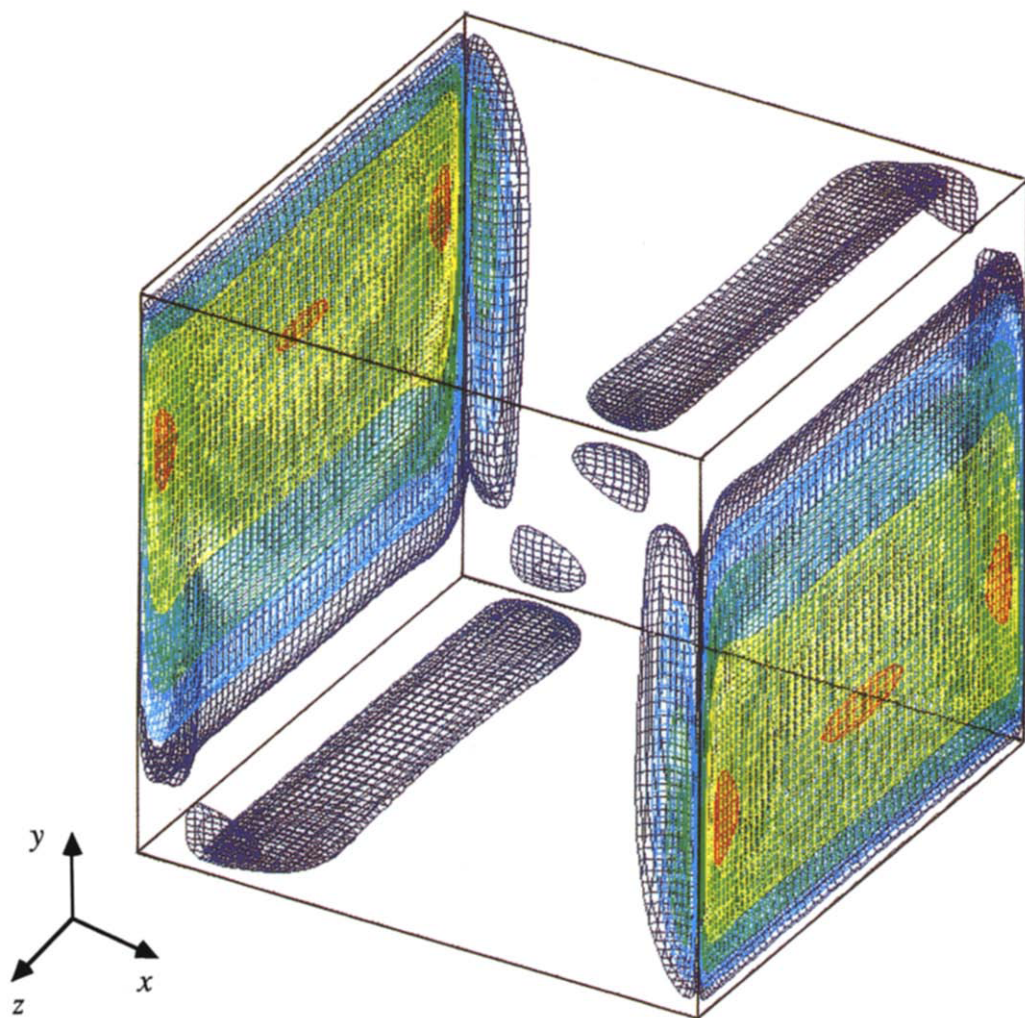


FIG. 7. Isosurfaces of the absolute values of the vorticity at $Ra = 10^6$ (contour levels: 3.6 (purple), 7.2 (blue), 10.8 (green), 14.4 (yellow), 18.0 (red)).

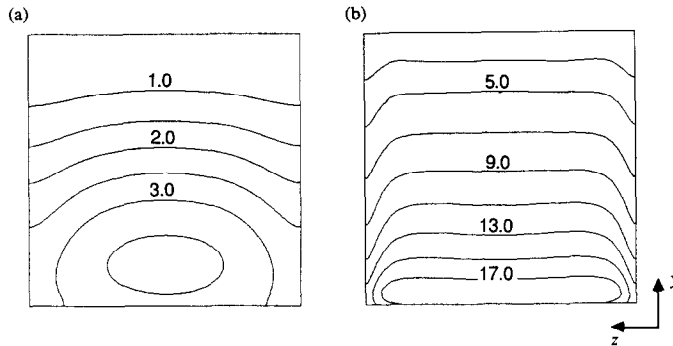


FIG. 8. Local Nusselt number distributions at the heated wall ($x = 1$): (a) $Ra = 10^4$; (b) $Ra = 10^6$.

$$Nu_{\text{mean}}(z) = \int_0^1 \frac{\partial T(y, z)}{\partial x} \Big|_{x=0 \text{ or } x=1} dy$$

$$\left(= \int_0^1 Nu_{\text{local}}(y, z) dy \right) \quad (7)$$

$$Nu_{\text{overall}} = \int_0^1 Nu_{\text{mean}}(z) dz. \quad (8)$$

Variations of the local Nusselt number at the heated wall ($x = 0$) are illustrated in Fig. 8 for the cases of $Ra = 10^4$ and 10^6 . At a high Rayleigh number ($Ra = 10^6$), the Nu_{local} distribution demonstrates prominent convection activities. The Nusselt number changes rapidly in the vertical direction. The z -variations of Nu_{local} are apparent only in the areas near the end walls ($z = 0$ and 1). The symmetric patterns are obtained for Nu_{local} at the cooled wall ($x = 0$, not shown).

Figure 9 represents the profiles of the mean Nusselt number along the z -direction at each Rayleigh number studied. For the Rayleigh numbers smaller than 10^5 , the mean Nusselt number increases as the symmetry plane is approached, and its peak value occurs at the symmetry plane located at $z = 0.5$. However, at $Ra = 10^6$ two minor peaks appear at $z = 0.2$ and 0.8 . The presence of the intense convective flow in the z -direction enhances the heat transfer in these regions at a high Rayleigh number.

The overall Nusselt number is tabulated in Table 1, and it is also illustrated in Fig. 8. In Table 1, the deviations from the two-dimensional predictions are also included. For the Rayleigh numbers smaller than 10^5 , the overall three-dimensional Nusselt numbers are found to be appreciably smaller than for the two-dimensional results. At $Ra = 10^6$, the difference is considerably small compared with the cases of lower Rayleigh numbers. This can be explained by noting that Nu_{overall} is almost uniform along the z -direction until it drops off sharply near the end walls for high Rayleigh numbers.

Utilizing the above numerical results, heat transfer correlations over $10^3 \leq Ra \leq 10^6$ for the three-dimensional enclosure are proposed as

$$Nu_{\text{mean}}(z = 0.5) = 0.1378 Ra^{0.304} \quad (9)$$

$$Nu_{\text{overall}} = 0.1307 Ra^{0.304}. \quad (10)$$

The above expressions give a maximum error of within 1% of the Nusselt number presented in Tables 1 and 2.

Characteristic field values in the symmetry plane ($z = 0.5$)

Comparisons of several important field variables in the symmetry plane ($z = 0.5$) with the two-dimensional data are attempted in this subsection. These will test the validity of the two-dimensional assumption, which has been routinely invoked for numerical studies. Table 2 reproduces the representative quantities of the flow field and the heat transfer rates in the symmetry plane. The differences between the two- and three-dimensional results are also indicated. The discrepancies in the local quantities (the peak velocities and the minimum and maximum Nusselt numbers) are as large as 10%, while those in the averaged quantity (the mean Nusselt number) are within 2%. In general, the changes are small at $Ra = 10^6$. At a high Rayleigh number, three-dimensionalities are insignificant in the bulk of the flow field, except in the regions near the end walls ($z = 0$ and 1), as previously remarked.

Comparison of the numerical predictions with the experimental measurements

As discussed in the previous section, several experimental studies have been conducted for the differentially heated cubical enclosure. In this subsection, comparison with the laboratory data is undertaken to verify the present numerical results. It is to be noted that, except for one set of measurements [11], enclosures with large depth aspect ratios ($A_z > 5$) were usually employed in the experiments; this precludes precise quantitative comparisons of each set of data.

Figure 10 represents the temperature distribution in the symmetry plane at $Ra = 10^5$. These numerical predictions are compared with the experimental data at $Ra = 1.89 \times 10^5$ acquired by a Mach-Zehnder interferometry technique [8]. The temperature profile

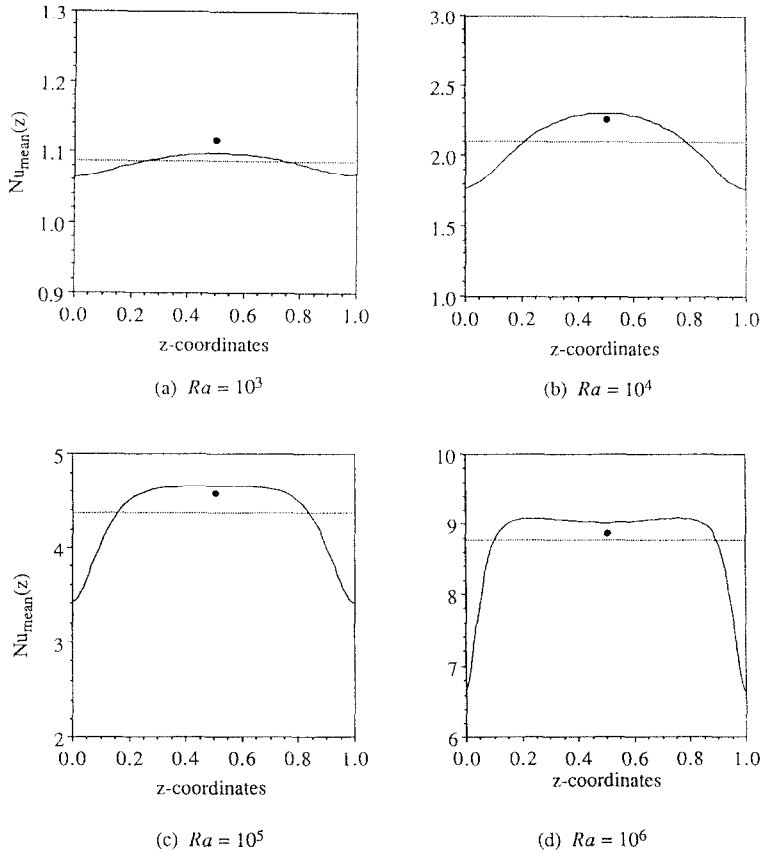


FIG. 9. Distribution of the mean Nusselt number in the z -direction (—, $Nu_{\text{mean}}(z)$ (three-dimensional); ····, Nu_{overall} ; ●, $Nu_{\text{mean}}(z)$ (two-dimensional)): (a) $Ra = 10^3$; (b) $Ra = 10^4$; (c) $Ra = 10^5$; (d) $Ra = 10^6$.

Table 1. The overall Nusselt number at the isothermal walls

Ra	10^3	10^4	10^5	10^6
Nu_{overall}	1.085(−4.52%)	2.100(−8.29%)	4.361(−4.75%)	8.770(−1.88%)

Note : the figures in parentheses indicate the difference between the three- and two-dimensional data.

Table 2. Representative field values in the symmetry plane ($z = 0.5$)

Ra	10^3	10^4	10^5	10^6
u_{max}	0.1314(−3.30%)	0.2013(4.47%)	0.1468(7.83%)	0.08416(5.60%)
y'	0.200	0.1833	0.1453	0.1443
v_{max}	0.1320(−4.39%)	0.2252(−3.95%)	0.2471(−5.18%)	0.2588(−1.31%)
x'	0.8333	0.8833	0.9353	0.9669
Nu_{max}	1.420(−5.85%)	3.652(3.12%)	7.795(2.45%)	17.67(1.13%)
y'	0.08333	0.6232	0.08256	0.03793
Nu_{min}	0.7639(4.45%)	0.6110(−2.00%)	0.7867(−9.06%)	1.257(−1.51%)
y'	1.0	1.0	1.0	1.0
Nu_{mean}	1.105(−2.62%)	2.302(1.22%)	4.646(1.68%)	9.012(0.854%)

Note : the figures in parentheses indicate the difference between the three- and two-dimensional data.

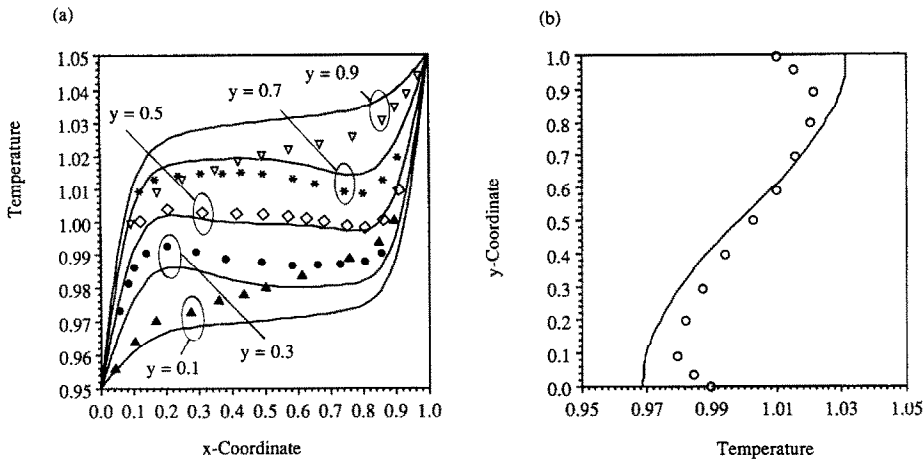


FIG. 10. Comparison of the temperature profiles in the symmetry plane at $z = 0.5$ ($Ra = 10^5$) (solid curves, present numerical results; symbols, measurements at $Ra = 1.89 \times 10^5$ [8]): (a) at various heights; (b) at $x = 0.5$.

at the mid-height ($y = 0.5$) agrees well with the measurements. The discrepancy between the computations and the measurements increases as the horizontal walls are approached. This may be attributed to the unavoidable heat transfer through the horizontal walls in the actual experimental situations. This is clearly observed in the measured temperature distribution at the enclosure center depicted in Fig. 10(b). In the experiments, the perfect insulator condition (which is routinely assumed in the numerical study) could not be strictly realized [8]. This is perhaps the reason for the discrepancy shown in Fig. 10(b).

Comparison of the velocity fields is shown for two Rayleigh numbers. Figure 11 illustrates the profiles of the horizontal and vertical velocity components at selected locations in the enclosure symmetry plane at $Ra = 10^5$. The velocity measurements by laser Doppler techniques (for $Ra = 1.03 \times 10^5$ [7] and 1.89×10^5

[8]) are also plotted in the same figure. The experimental data of Krane and Jessee [8], at a slightly higher Rayleigh number than that considered in the present computation, agree reasonably well with the numerical predictions. Slight deviations are found in the peak values of the vertical velocity (v) near the isothermal walls and in the locations where they occur, as well as in the values of the peaks of the horizontal velocity. These may reflect the effects of intensified convective activities at a higher Rayleigh number. The results of Bilski *et al.* [7] exhibit considerable asymmetry in the profiles even though the overheat ratio of their experiments is small, $\delta < 0.03$. When the overheat ratio is large ($\delta > 0.2$), the effects of the non-uniform fluid properties may have a measurable impact on the field characteristics; thus, the asymmetric fields will be formed, as reported in the two-dimensional numerical studies for differentially

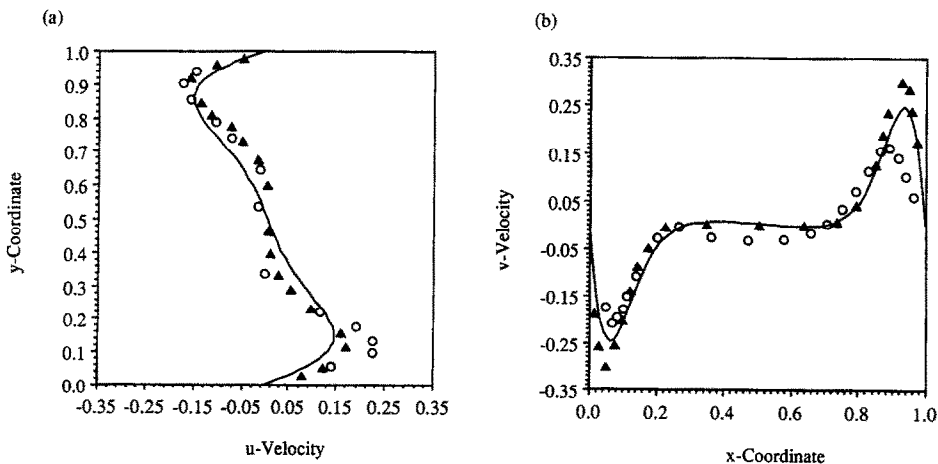


FIG. 11. Comparison of the velocity profiles in the symmetry plane at $z = 0.5$ ($Ra = 10^5$) (solid curves, present numerical results; \circ , measurements at $Ra = 1.03 \times 10^5$ [7]; \blacktriangle , measurements at $Ra = 1.89 \times 10^5$ [8]): (a) at $x = 0.5$; (b) at $y = 0.5$.

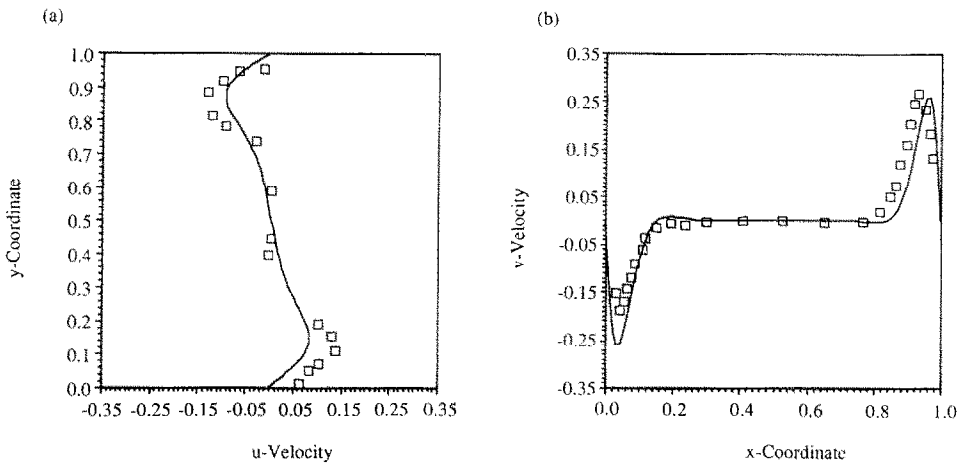


Fig. 12. Comparison of the velocity profiles in the symmetry plane at $z = 0.5$ ($Ra = 10^6$) (solid curves, present numerical results; \square , measurements at $Ra = 1.13 \times 10^6$ [7]): (a) at $x = 0.5$; (b) at $y = 0.5$.

heated square enclosures [17–19]. No clear explanations were given in ref. [7] as to the cause of the asymmetric velocity profiles, which appeared at the small overheat ratio used.

The horizontal velocity (u) profiles of both experiments indicate the existence of a region of very low velocities near the mid-height of the enclosure. This is not quite evident in the numerical predictions, in which the velocity changes gradually from a peak to another peak almost linearly. The effects of the extraneous heat transfer through the horizontal walls in the experiments could be the sources of the discrepancy [6–8].

The results at $Ra = 10^6$ are shown in Fig. 12, in which the experimental data obtained by Bilski *et al.* [7] for $Ra = 1.13 \times 10^6$ are included. Again, at this Rayleigh number, the asymmetry of the profiles is noticeable in the measurements. However, the degree of the asymmetry decreased in comparison to the case of the lower Rayleigh number discussed previously. The experimental results overpredict the peak values of the horizontal velocity components compared to the numerical results, while they show reasonable agreement for the vertical velocity profiles.

CONCLUSIONS

In the present numerical study, three-dimensional steady flow analyses have been made on natural convection in a differentially heated cubical enclosure. The detailed structures of the three-dimensional fields were scrutinized by using high-resolution computational results over the range of Rayleigh numbers studied, $10^3 \leq Ra \leq 10^6$.

Examinations of the perspective three-dimensional fields revealed that the variations in the z -direction were evident particularly near the end walls ($z = 0$ and 1). As the Rayleigh number increases, the convective activities intensify, and significant z -variations tend to be confined into narrower areas close to the end walls.

The w velocity was found to be an order of mag-

nitude smaller than the dominant velocities (u and v) over the entire Rayleigh number range studied. The non-zero values of the w velocity were noticed in the end wall regions, specifically near the corners. The size of these areas becomes smaller as Ra increases. At high Rayleigh numbers, the secondary vortices form along the vertical edges; these affect the mean Nusselt number distribution.

The predicted overall Nusselt numbers show considerable discrepancies from the corresponding two-dimensional solutions. The maximum difference was found to occur near $Ra = 10^4$, which is near the transition point between the conduction dominant flow and the boundary layer-type flow structure.

The present three-dimensional data are found to be in fair consistency with the available experimental measurements. Comparisons with the prior experimental results for air suggest that the thermal boundary condition at the horizontal walls has a considerable influence on the vertical profiles of flow variables.

Note: the interested reader should contact the first author for the quantitative results of these three-dimensional computations.

Note added to proof—It has come to our attention that a similar work was recently performed by using the finite element method.

D. W. Pepper, Modeling of three-dimensional natural convection with a time-split finite-element technique, *Numer. Heat Transfer* **11**, 31–55 (1987).

Acknowledgement—The authors are grateful to Dr Elaine S. Oran of the Naval Research Laboratory, Washington, DC, for her discussions and comments.

REFERENCES

1. N. C. Markatos and K. A. Pericleous, Laminar and turbulent natural convection in an enclosed cavity, *Int. J. Heat Mass Transfer* **27**, 755–772 (1984).
2. G. de Vahl Davis, Natural convection of air in a square cavity: a bench mark numerical solution, *Int. J. Numer. Meth. Fluids* **3**, 249–264 (1983).

3. G. D. Mallinson and G. de Vahl Davis, Three-dimensional natural convection in a box: a numerical study, *J. Fluid Mech.* **83**, 1–31 (1977).
4. T. S. Lee, G. H. Son and J. S. Lee, Numerical predictions of three-dimensional natural convection in a box, *Proc. 1st KSME-JSME Thermal and Fluids Engng Conf.*, Vol. 2, pp. 278–283 (1988).
5. A. M. Lankhorst and C. J. Hoogendoorn, Three-dimensional numerical calculations of high Rayleigh number natural convective flows in enclosed cavities, *Proc. 1988 Natn. Heat Transfer Conf.*, ASME HTD-96, Vol. 3, pp. 463–470 (1988).
6. S. M. Bajorek and J. R. Lloyd, Experimental investigation of natural convection in partitioned enclosures, *J. Heat Transfer* **104**, 527–532 (1982).
7. S. M. Bilski, J. R. Lloyd and K. T. Yang, An experimental investigation of the laminar natural convection velocity in square and partitioned enclosures, *Proc. 8th Int. Heat Transfer Conf.*, Vol. 4, pp. 1513–1518 (1986).
8. R. J. Krane and J. Jessee, Some detailed field measurements for a natural convection flow in a vertical square enclosure, *Proc. 1st ASME-JSME Thermal Engng Joint Conf.*, Vol. 1, pp. 323–329 (1983).
9. D. G. Briggs and D. N. Jones, Two-dimensional periodic natural convection in a rectangular enclosure of aspect ratio one, *J. Heat Transfer* **107**, 850–854 (1985).
10. M. S. Bohn, A. T. Kirkpatrick and D. A. Olson, Experimental study of three-dimensional natural convection high-Rayleigh number, *J. Heat Transfer* **106**, 339–345 (1984).
11. W. J. Hiller, S. Koch, T. A. Kowalewski, G. de Vahl Davis and M. Behnia, Experimental and numerical investigations of natural convection in a cube with two heated side walls, *Proc. IUTAM Symp.*, pp. 717–726 (1990).
12. S. V. Patankar, *Numerical Heat Transfer and Fluid Flow*, Chap. 6. Hemisphere, Washington, DC (1980).
13. H. L. Stone, Iterative solution of implicit approximations of multi-dimensional partial differential equations, *J. Numer. Analysis* **5**, 530–558 (1968).
14. B. P. Leonard, A stable and accurate convection modeling procedure based on quadratic upstream interpolation, *Comput. Meth. Appl. Mech. Engng* **19**, 59–98 (1979).
15. C. J. Freitas, R. L. Street, A. N. Findikakis and J. R. Koseff, Numerical simulation of three-dimensional flow in a cavity, *Int. J. Numer. Meth. Fluids* **5**, 561–575 (1985).
16. S. Shirayama and K. Kuwahara, Patterns of three-dimensional boundary layer separation, 25th Aerospace Sciences Meeting, AIAA Paper 87-0461 (1987).
17. E. Leonardi and J. A. Reizes, Convective flows in closed cavities with variable fluid properties. In *Numerical Methods in Heat Transfer* (Edited by R. W. Lewis, K. Morgan and O. C. Zienkiewicz), Chap. 18. Wiley, New York (1981).
18. Z. Y. Zhong, K. T. Yang and J. R. Lloyd, Variable property effects in laminar natural convection in a square enclosure, *J. Heat Transfer* **107**, 133–138 (1985).
19. J. M. Hyun and J. W. Lee, Transient natural convection in a square cavity of a fluid with temperature-dependent viscosity, *Int. J. Heat Fluid Flow* **9**, 278–285 (1988).

ETUDE NUMERIQUE DE LA CONVECTION TRIDIMENSIONNELLE DANS UNE CAVITE CUBIQUE CHAUFFEE DIFFERENTIELLEMENT

Résumé—On rapporte une étude numérique, par différences finies à haute résolution, de la convection naturelle permanente tridimensionnelle de l'air pour un nombre de Rayleigh $10^3 \leq Ra \leq 10^6$, dans une cavité cubique dont deux parois verticales sont chauffées différentiellement. On décrit les détails de l'écoulement tridimensionnel et des caractéristiques thermiques. On utilise les visualisations graphiques de l'écoulement. L'existence de la composante de vitesse selon z , est clairement visible bien que de faible valeur. On fait la comparaison des présents résultats tridimensionnels avec les solutions bidimensionnelles.

Les premiers montrent un accord raisonnable avec les mesures expérimentales.

NUMERISCHE UNTERSUCHUNG DER DREIDIMENSIONALEN KONVEKTION IN EINEM UNGLEICHMÄSSIG BEHEIZTEN WÜRFELFÖRMIGEN HOHLRAUM

Zusammenfassung—Die stationäre, dreidimensionale natürliche Konvektion von Luft in einem würfelförmigen Hohlraum, in dem zwei Seitenwände unterschiedlich beheizt werden, wird mit Hilfe eines hochauflösenden Differenzenverfahrens im Bereich $10^3 \leq Ra \leq 10^6$ numerisch untersucht. Die dreidimensionale Strömung und die thermischen Vorgänge werden eingehend beschrieben. Dazu werden moderne Verfahren der Sichtbarmachung von berechneten Strömungen eingesetzt. Das Vorhandensein einer Geschwindigkeitskomponente in z -Richtung wird nachgewiesen, obwohl diese sehr klein ist. Die Ergebnisse dieser dreidimensionalen Berechnungen werden mit denen zweidimensionaler Verfahren verglichen. Die dreidimensionalen Berechnungen stimmen gut mit Versuchswerten überein.

ЧИСЛЕННОЕ ИССЛЕДОВАНИЕ ТРЕХМЕРНОЙ КОНВЕКЦИИ В НЕОДНОРОДНО НАГРЕВАЕМОЙ КУБИЧЕСКОЙ ПОЛОСТИ

Аннотация—Приводятся результаты численного исследования конечно-разностным методом высокого разрешения трехмерной стационарной естественной конвекции воздуха при значениях числа Рэлея, изменяющихся в интервале $10^3 \leq Ra \leq 10^6$, в кубической полости с двумя различно нагреваемыми вертикальными стенками. Описываются детали трехмерного течения и тепловые характеристики. Широко применяются современные численные методы визуализации течения. Четко показывается наличие поперечной компоненты скорости несмотря на ее малую величину. Проводится сравнение полученных трехмерных результатов с двумерными решениями. Трехмерные результаты демонстрируют удовлетворительное согласие с экспериментальными данными.